



# MIT Open Access Articles

## *Lower hybrid current drive at high density in Alcator C-Mod*

The MIT Faculty has made this article openly available. **Please share** how this access benefits you. Your story matters.

<b>Citation</b>	Wallace, G.M. et al. "Lower Hybrid Current Drive at High Density in Alcator C-Mod." Nuclear Fusion 51.8 (2011): 083032.
<b>As Published</b>	<a href="http://dx.doi.org/10.1088/0029-5515/51/8/083032">http://dx.doi.org/10.1088/0029-5515/51/8/083032</a>
<b>Publisher</b>	IOP Publishing
<b>Version</b>	Author's final manuscript
<b>Citable link</b>	<a href="http://hdl.handle.net/1721.1/81774">http://hdl.handle.net/1721.1/81774</a>
<b>Terms of Use</b>	Creative Commons Attribution-Noncommercial-Share Alike 3.0
<b>Detailed Terms</b>	<a href="http://creativecommons.org/licenses/by-nc/3.0">http://creativecommons.org/licenses/by-nc/3.0</a>

**PSFC/JA-10-55**

**Lower Hybrid Current Drive at High Density in Alcator  
C-Mod**

G.M. Wallace, A.E. Hubbard, P.T. Bonoli, I.C. Faust,  
R.W. Harvey\*, J.W. Hughes, B.L. LaBombard, O.  
Meneghini, R.R. Parker, A.E. Schmidt, S. Shiraiwa,  
A.P. Smirnov\*, D.G. Whyte, J.R. Wilson\*\*, J.C. Wright,  
S.J. Wukitch, and the Alcator C-Mod Team

January 2011

**Plasma Science and Fusion Center  
Massachusetts Institute of Technology  
Cambridge, MA 02139 USA**

**\* CompX**

**Del Mar, CA 92104 USA**

**\*\* Princeton Plasma Physics Laboratory  
Princeton, NJ 08543 USA**

This work was supported by the U.S. Department of Energy awards DE-FC02-99ER54512 and DE-AC02-76CH03073. Reproduction, translation, publication, use and disposal, in whole or in part, by or for the United States government is permitted.

Submitted for publication to *Nuclear Fusion*.

# Lower Hybrid Current Drive at High Density in Alcator C-Mod

G.M. Wallace 1), A.E. Hubbard 1), P.T. Bonoli 1), I.C. Faust 1), R.W. Harvey 2), J.W. Hughes 1), B.L. LaBombard 1), O. Meneghini 1), R.R. Parker 1), A.E. Schmidt 1), S. Shiraiwa 1), A.P. Smirnov 2), D.G. Whyte 1), J.R. Wilson 3), J.C. Wright 1), S.J. Wukitch 1), and the Alcator C-Mod Team

1) MIT Plasma Science and Fusion Center, Cambridge, MA 02139, USA 2) CompX, Del Mar, CA 92014, USA 3) Princeton Plasma Physics Laboratory, Princeton, NJ 08543, US

E-mail: wallaceg@mit.edu

**Abstract.** Experimental observations of lower hybrid current drive (LHCD) at high density on the Alcator C-Mod tokamak are presented in this paper. Bremsstrahlung emission from relativistic fast electrons in the core plasma drops suddenly above line averaged densities of  $10^{20} \text{ m}^{-3}$  ( $\omega/\omega_{LH} \sim 3$ ) in single null discharges with large ( $> 10 \text{ mm}$ ) plasma-inner wall gaps, well below the density limit previously observed on limited tokamaks ( $\omega/\omega_{LH} \sim 2$ ). Modeling and experimental evidence suggest that the absence of LHCD driven fast electrons at high density may be due to parasitic collisional absorption in the scrape off layer. Experiments show that the population of fast electrons produced by LHCD at high density ( $\bar{n}_e > 10^{20} \text{ m}^{-3}$ ) can be increased significantly by operating with a plasma-inner wall gap of less than  $\sim 5 \text{ mm}$  with the strongest non-thermal emission in inner-wall limited plasmas. A change in plasma topology from single to double null produces a modest increase in non-thermal emission at high density. Increasing the electron temperature in the periphery of the plasma ( $0.8 > r/a > 1.0$ ) also results in a modest increase in non-thermal electron emission above the density limit. Ray tracing/Fokker-Planck simulations of these discharges predict the observed sensitivity to plasma position when the effects of collisional absorption in the SOL are included in the model.

PACS numbers: 52.35.Hr, 52.50.Sw, 52.55.Wq

## 1. Introduction

Tokamak experiments require a toroidal current to provide plasma confinement. This toroidal current is conventionally driven by transformer action, although relying solely on inductive current drive limits the maximum duration of the pulse. Lower hybrid (LH) waves can be used on tokamak experiments as a means of generating non-inductive current [1]. Lower hybrid current drive (LHCD) is a particularly attractive method of driving non-inductive current due to its high current drive efficiency,  $\eta = n_e I_P R_0 / P_{LH} \sim 0.1 \times 10^{20} \text{ m}^{-2} \text{ MW}^{-1} \text{ MA}$ , and ability to drive current off axis.

The LHCD system [2] on the Alcator C-Mod tokamak [3] is designed to investigate current profile control under plasma conditions relevant to future devices such as ITER and DEMO. This paper addresses the behavior of Lower Hybrid (LH) waves in a compact, high field, high density, diverted tokamak. The C-Mod LHCD system has demonstrated efficient current drive at line averaged densities below  $1 \times 10^{20} \text{ m}^{-3}$  [4], however the current drive efficiency in single null discharges is substantially reduced above the “density limit” of  $\bar{n}_e \sim 1 \times 10^{20} \text{ m}^{-3}$  [5, 6, 7, 8]. This critical density associated with reduced current drive in the core plasma on C-Mod is unusual in that it occurs at a density significantly lower ( $\omega/\omega_{LH} \sim 3 - 4$ ) than what would have been expected based on scaling laws from prior LHCD experiments ( $\omega/\omega_{LH} \sim 2$ ) [9, 10]. Here,  $\omega_{LH} \approx \omega_{pi}^2 / (1 + \omega_{pe}^2 / \omega_{ce}^2)$  is the lower hybrid frequency and  $\omega = 2\pi \times 4.6 \text{ GHz}$  is the launched wave frequency. Experimental results suggest that interactions between LH waves and the scrape off layer (SOL) plasma can have a substantial impact on the operational effectiveness of a LHCD system at high density.

Bremsstrahlung emission in the 50-200 keV range can be taken as a proxy for the population of fast electrons generated by LHCD. Bremsstrahlung on C-Mod is diagnosed with a 32-chord hard x-ray (HXR) camera [11] with simultaneous spatial, temporal, and energy resolving capabilities. Through experiments conducted during the 2008 run campaign, it was discovered that, for single null discharges with line averaged densities in excess of  $10^{20} \text{ m}^{-3}$ , the fast electron bremsstrahlung emissivity (and thus the population of fast electrons carrying the non-inductive current) was 2-3 orders of magnitude lower than is predicted by a fast electron bremsstrahlung synthetic diagnostic in the ray tracing/Fokker-Planck solver package GENRAY/CQL3D [12, 13, 14]. Figure 1 shows that the experimental HXR data (small symbols) diverges from the  $1/\bar{n}_e$  trend predicted by the CQL3D synthetic diagnostic (solid line) for  $\bar{n}_e > 10^{20} \text{ m}^{-3}$ . Current drive efficiency is also predicted to scale as  $1/n_e$  based on a simple theoretical model [1, 15]. The LHCD system is capable of driving 570 kA of current with zero loop voltage at  $\bar{n}_e = 0.5 \times 10^{20} \text{ m}^{-3}$  [16], while no signs of current drive are evident at  $\bar{n}_e = 1.5 \times 10^{20} \text{ m}^{-3}$ . This limit for production of non-thermal electrons by LHCD is observed at a significantly lower density than was expected based on previous results from other experiments for which wave accessibility (i.e. mode conversion from the slow wave to the fast wave) or parametric decay instabilities set the LHCD density limit. The insensitivity of the observed density limit to changes in magnetic field and launched  $n_{||}$

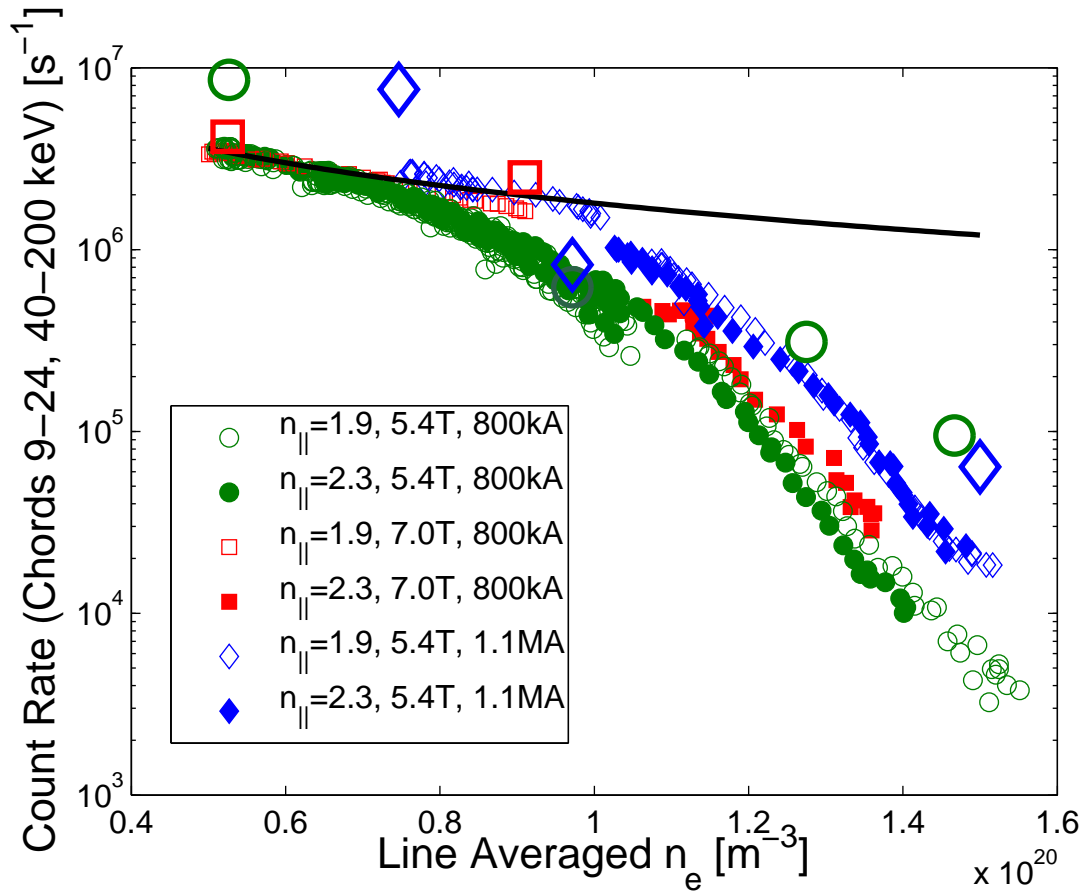


**Figure 1.** Comparison of fast electron bremsstrahlung emission predicted by GENRAY/CQL3D code package with a 2-dimensional SOL model in GENRAY including the effects of collisional damping in the SOL. Experimental count rates have been normalized to  $P_{LH}^{0.5}$ . The large symbols represent simulations while the small symbols are experimental data. The solid line represents a  $1/n_e$  trend as predicted by GENRAY/CQL3D without a SOL. All discharges plotted are single null.

also eliminates these phenomena as as possible explanations for the C-Mod results.

Parallel electric currents in the SOL are observed during high power LHCD at high density. The direction of the SOL currents for lower- and upper-single-null configurations is the same as the plasma current inside the last closed flux surface (LCFS). Equal and opposite SOL currents are measured on the inner and outer divertors, with the circuit completed through the vacuum vessel wall. The magnitude of the SOL current increases rapidly across the same range of densities for which the core X-ray emission drops, i.e.  $\bar{n}_e > 1 \times 10^{20} \text{ m}^{-3}$ . The increase in SOL current is well correlated with an increase in ion saturation current,  $I_{sat}$ , and thus plasma density, at the ion collecting end of the field line. A modification of density in the SOL of this magnitude indicates strong absorption of the LH waves outside the LCFS.

The core bremsstrahlung and SOL current observations suggest that power absorption is shifting from inside the LCFS into the SOL as density increases. By

including collisional absorption of the LH waves [17] and a SOL in the ray tracing model, agreement between modeling and experimental results is dramatically improved at high density [5, 6, 7]. Figure 1 shows a comparison between the experimental data and the model including absorption in the SOL. The observed density limit on C-Mod appears to be a consequence of poor ray penetration to the hot plasma core and weak single pass absorption inside the LCFS, combined with a loss mechanism in the SOL such as collisional damping.

## 2. Sensitivity to Plasma Topology

Experiments during the 2010 campaign on C-Mod show that plasma topology plays an important and unexpected role in the LHCD density limit. Figure 2 shows the line integrated HXR emission for upper single null (USN), lower single null (LSN), double null (DN), and inner wall limited discharges on C-Mod. HXR emission increases by two orders of magnitude at  $\bar{n}_e \sim 1.5 \times 10^{20} \text{ m}^{-3}$  in limited discharges (stars) as compared to single null (circles), and an increase of nearly an order of magnitude in double null (triangles). The HXR emission in limited discharges lies on the  $1/\bar{n}_e$  trend line as predicted by GENRAY/CQL3D when run without a SOL. This  $1/\bar{n}_e$  trend extends up to a value of at least  $1.6 \times 10^{20} \text{ m}^{-3}$  (the highest  $\bar{n}_e$  explored to date). Above this density the accessibility of the LH waves is expected to be marginal (i.e. the slow and fast wave roots of the dispersion relation may coalesce). HXR emission in DN configuration deviates from the  $1/\bar{n}_e$  trend above  $\bar{n}_e \sim 1 \times 10^{20} \text{ m}^{-3}$ , although not as steeply as in lower null. Non-thermal electron cyclotron emission (ECE) trends similarly as a function of  $\bar{n}_e$  and configuration.

The double null discharges were fueled both by high field side (HFS) and low field side (LFS) gas puffing, although no clear difference in bremsstrahlung emission is seen between the two gas puffing locations. The single null and limited discharges were fueled on the LFS. The elongation of high density inner wall limited discharges was varied from  $\kappa = 1.15$  to  $\kappa = 1.5$  to determine if plasma shaping has an effect on the density limit. These experiments showed that HXR emission in limited discharges is not sensitive to changes in plasma elongation.

Reciprocating Langmuir probe measurements of the SOL electron density profiles in high density ( $\bar{n}_e \sim 1.3 \times 10^{20} \text{ m}^{-3}$ ) discharges show a significant difference between limited and diverted configurations. The SOL  $n_e$  profiles for limited and LSN discharges are plotted in Figure 3. There is a small increase in SOL density during LH for the limited case, particularly for  $\rho > 15 \text{ mm}$ . The changes in the SOL density profile during LH in LSN are much more dramatic. The density at  $\rho = 20 \text{ mm}$  increases by an order of magnitude during LH. The increase in density in the far SOL is so severe that the profile is non-monotonic. The SOL  $T_e$  profiles do not change significantly during LH in either configuration. Some of the LH power may be channeled into sustaining the increased density in the far SOL for both the limited and LSN discharges, although the power required to generate the density profile changes in the LSN case would be larger

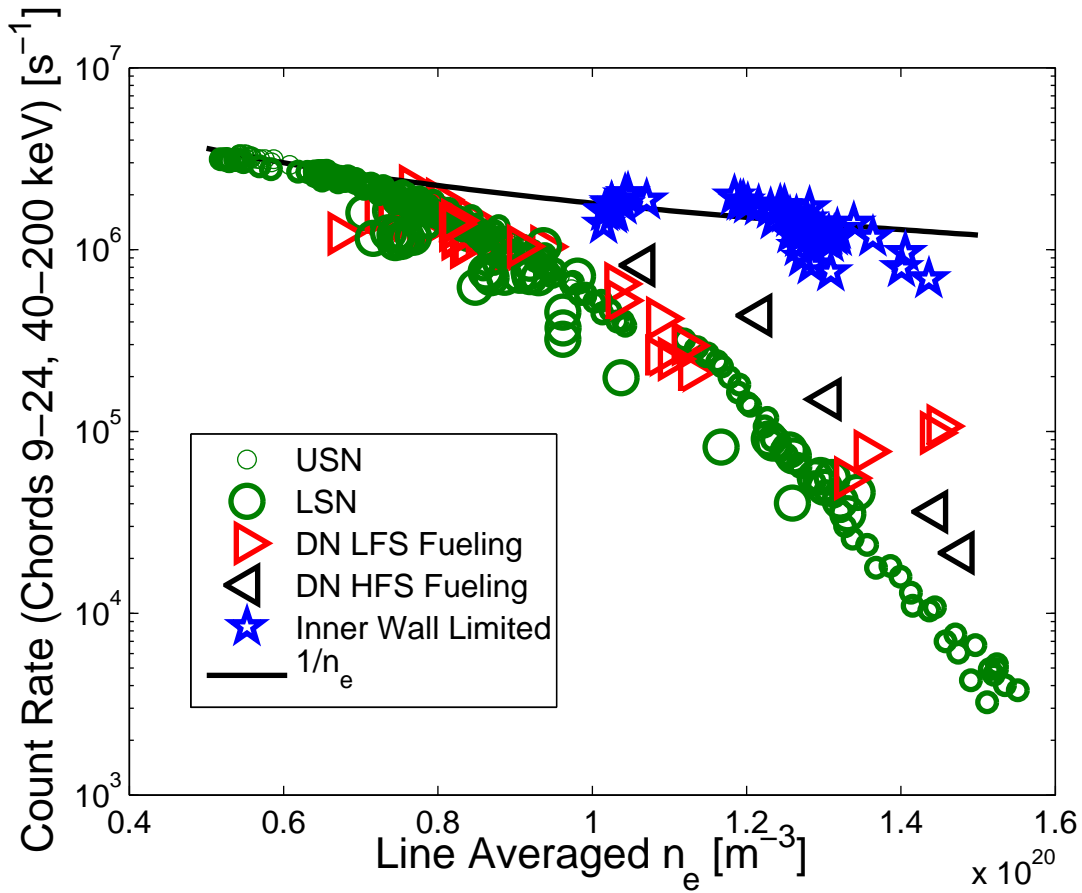


**Figure 2.** Comparison of fast electron bremsstrahlung emission as a function of density for different plasma topologies. Double null and particularly limited discharges show a significant increase in fast electron bremsstrahlung over single null discharges. The solid line represents a  $1/n_e$  trend. All discharges plotted are at 800 kA and 5.4 T. Diverted discharges have plasma–inner wall gaps greater than 10 mm.

than for the limited case based on the magnitude of the density increase.

### 3. Sensitivity to Plasma–Inner Wall Gap

The plasma–inner wall gap was systematically scanned in upper null discharges to determine the threshold inner gap for increased HXR emission. Dynamic scans of the inner gap in both directions (inner wall limited to USN and USN to inner wall limited) show that HXR emission is nearly constant for inner gaps greater than  $\sim 5$  mm, and that HXR emission is anti-correlated with inner gap below  $\sim 5$  mm. Figure 4 shows the time evolution of two discharges with dynamic inner gap scans. Although the line averaged density varies slightly during LHCD, non-thermal emission is clearly higher for plasma–inner wall gaps of less than  $\sim 5$  mm.

Figure 5 shows HXR emission as a function of density for plasma–inner wall gaps of 10–15 mm, 3–5 mm, and 0 mm (i.e. inner wall limited). Some of the increase in HXR

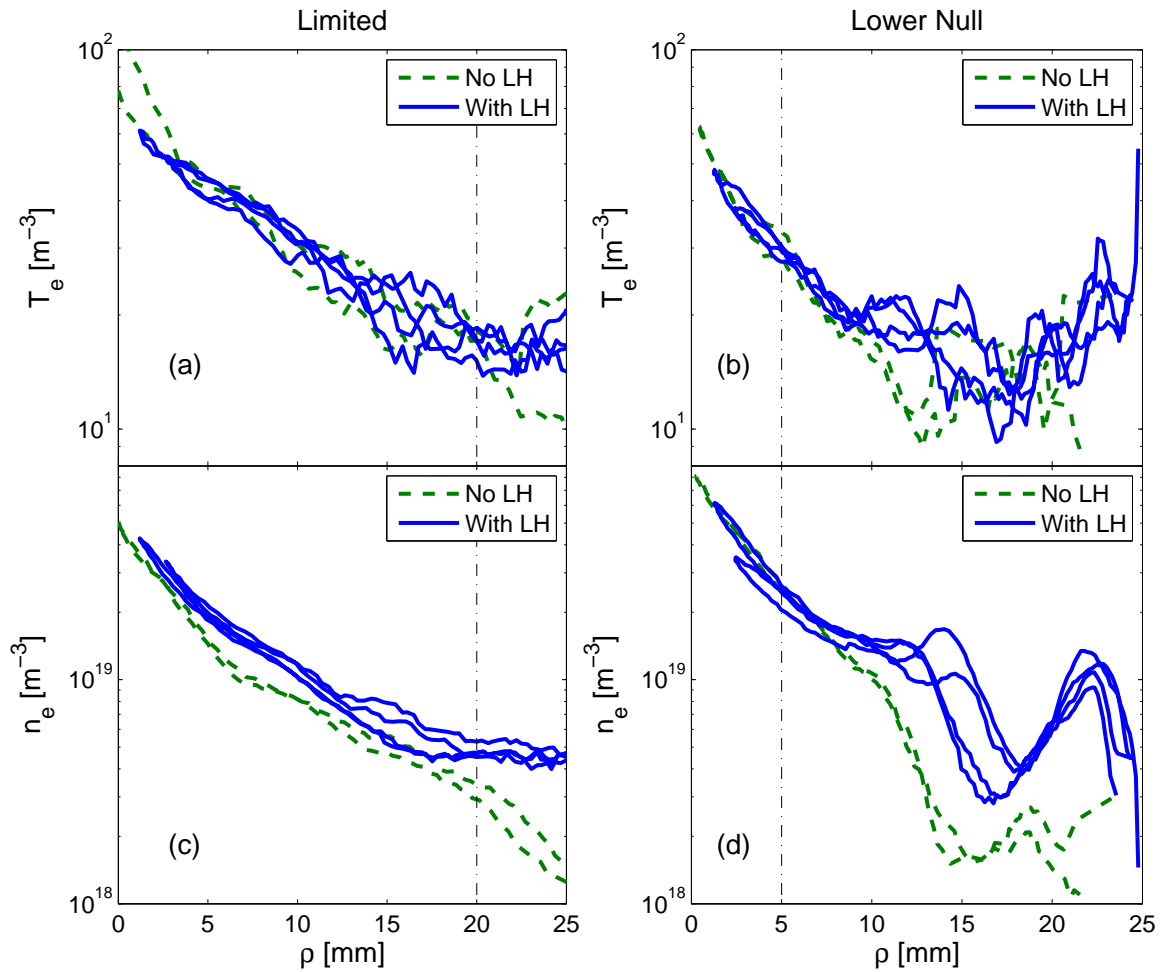


**Figure 3.** Electron temperature and density profiles in the SOL of high density ( $\bar{n}_e \sim 1.3 \times 10^{20} \text{ m}^{-3}$ ) with and without LH for (a/c) inner-wall limited and (b/d) LSN discharges. The density profiles are plotted as functions of  $\rho \equiv R - R_{LCFS}$  on the midplane. A single in-out sweep before LH and two in-out sweeps during LH are shown for both configurations. Limited discharges exhibit a noticeable increase in density for  $\rho > 15$  mm. The density profile in the far SOL increases more dramatically during LH in LSN discharges. Vertical dash-dot lines indicate the position of the low field side plasma limiter for each discharge. Both discharges are at 800 kA, 5.4 T.

emission at zero plasma–inner wall gap can be explained by an increase in  $Z_{eff}$  in limited discharges or by thick-target bremsstrahlung from fast electrons striking the inner wall. The non-thermal ECE, which is not sensitive to  $Z_{eff}$  or thick target bremsstrahlung, also shows an increase in the population of non-thermal LH generated electrons as the plasma–inner wall gap decreases (see Figure 6).

High density single null discharges with small inner gaps do exhibit signs of current drive despite weaker non-thermal emission as compared to inner wall limited discharges. Two discharges with the same net LH power (650 kW), plasma current (800 kA), toroidal



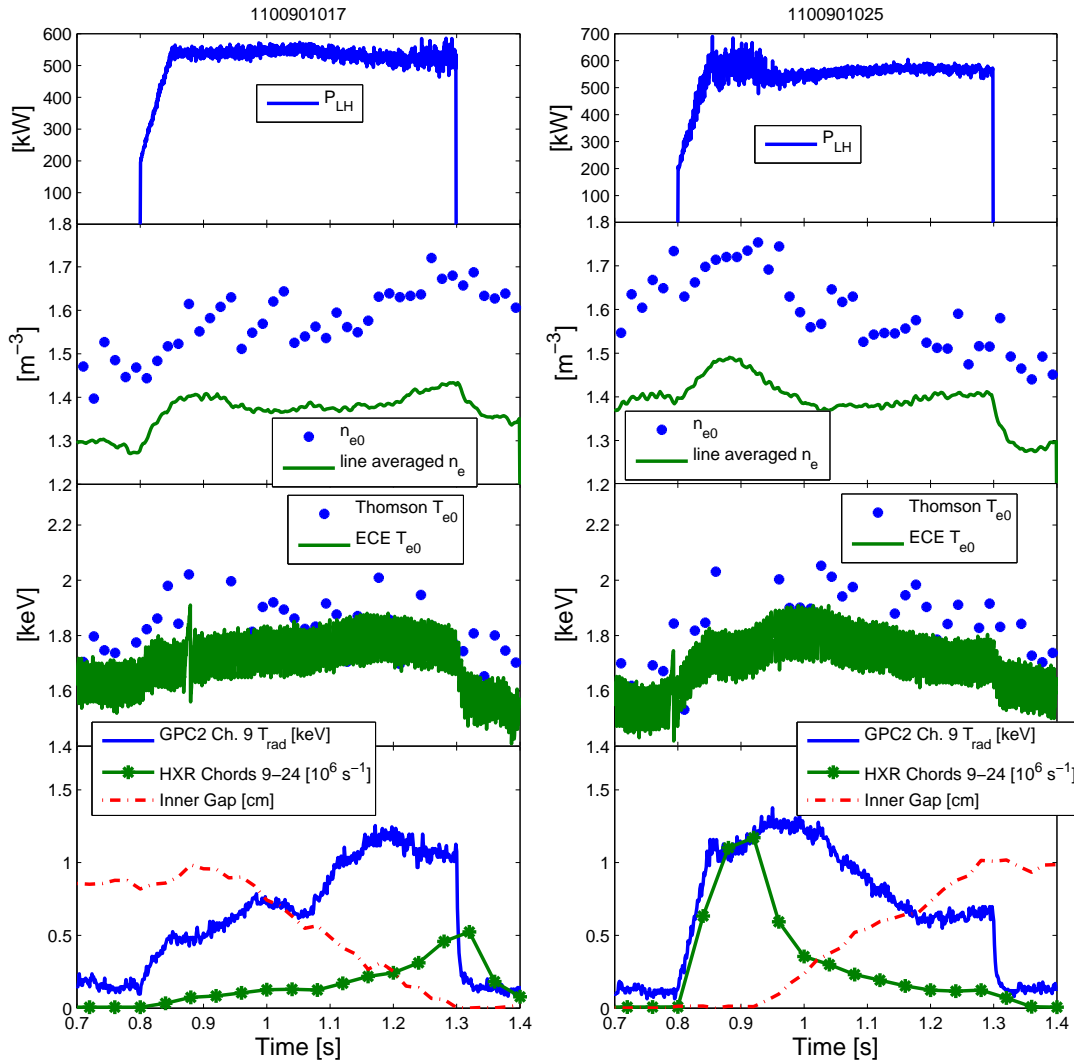


**Figure 4.** Plasma evolution during plasma–inner wall gap scans in single null. ECE and HXR emission are anti-correlated with inner gap for gaps below  $\sim 5$  mm. HXR emission is not sensitive to inner gaps greater than  $\sim 5$  mm. GPC2 Channel 9 (bottom panels) primarily measures non-thermal emission. Both discharges are at 800 kA, 5.4 T.

field (5.4 T), and line averaged density ( $\bar{n}_e = 1.3 \times 10^{20} \text{ m}^{-3}$ ) but different inner wall gaps (0 mm as compared to 4 mm) both show improved current drive performance over typical single null discharges (10–15 mm inner wall gaps). The relative change in loop voltage during LHCD,  $\Delta V/V$ , for the limited discharge was 0.17, while the relative change in loop voltage was 0.12 for the USN discharge with an inner gap of 4 mm. Non-thermal ECE and HXR emission is approximately double in the limited discharge as compared to the small gap discharge.

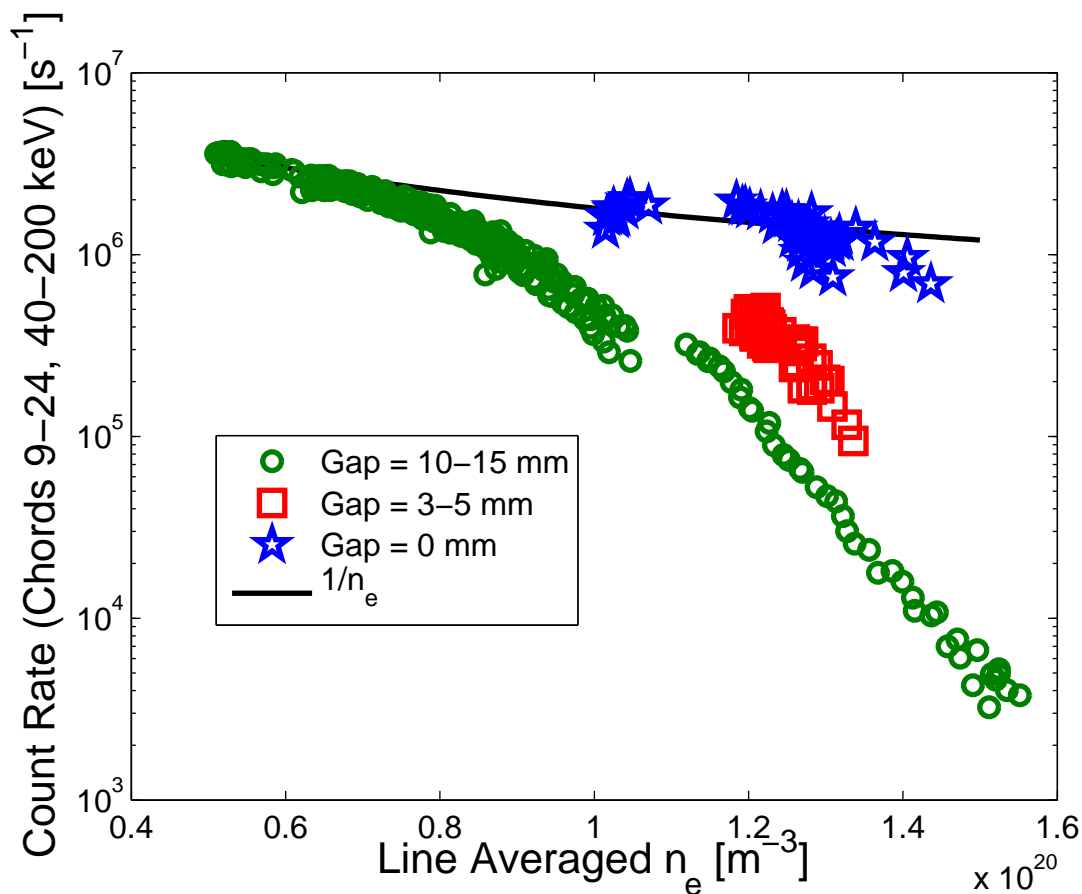


**Figure 5.** Comparison of fast electron bremsstrahlung emission as a function of density for different plasma–inner wall gaps. The solid line represents a  $1/n_e$  trend. All discharges plotted are 800 kA, 5.4 T.

#### 4. Sensitivity to Plasma Temperature

The results discussed in the preceding sections were obtained in L-mode discharges with LH the only additional heating. The low temperature of these discharges results in a low single-pass absorption regime for the LH waves. It was hoped that by increasing the plasma temperature, and thus the damping of the rays on the first pass through the plasma, that the effect of parasitic edge losses would be reduced. The central electron temperatures of L-mode plasma targets ( $\bar{n}_e = 1.2 - 1.45 \times 10^{20} \text{ m}^{-3}$ ,  $I_p = 1.1 \text{ MA}$ ,  $B_t = 5.4 \text{ T}$ ) were raised by applying 1.0, 2.0, and 2.5 MW of ion cyclotron range of frequency (ICRF) minority heating at 78 and 80 MHz. The temperature profiles in the discharges with ICRF were highly peaked and  $T_{r/a=0.9}$  was in the range of 200–400 eV. These discharges exhibited an increase in  $T_{e0}$  from 2 keV for the ohmic targets to over 4 keV with 2.5 MW of ICRF. Figure 7 shows a comparison between temperature profiles for discharges with ICRF and LH as compared to a discharge with only LH.

The HXR count rates show little increase with ICRF heating in L-mode, although it should be noted that high power ICRF causes a large increase in the background HXR

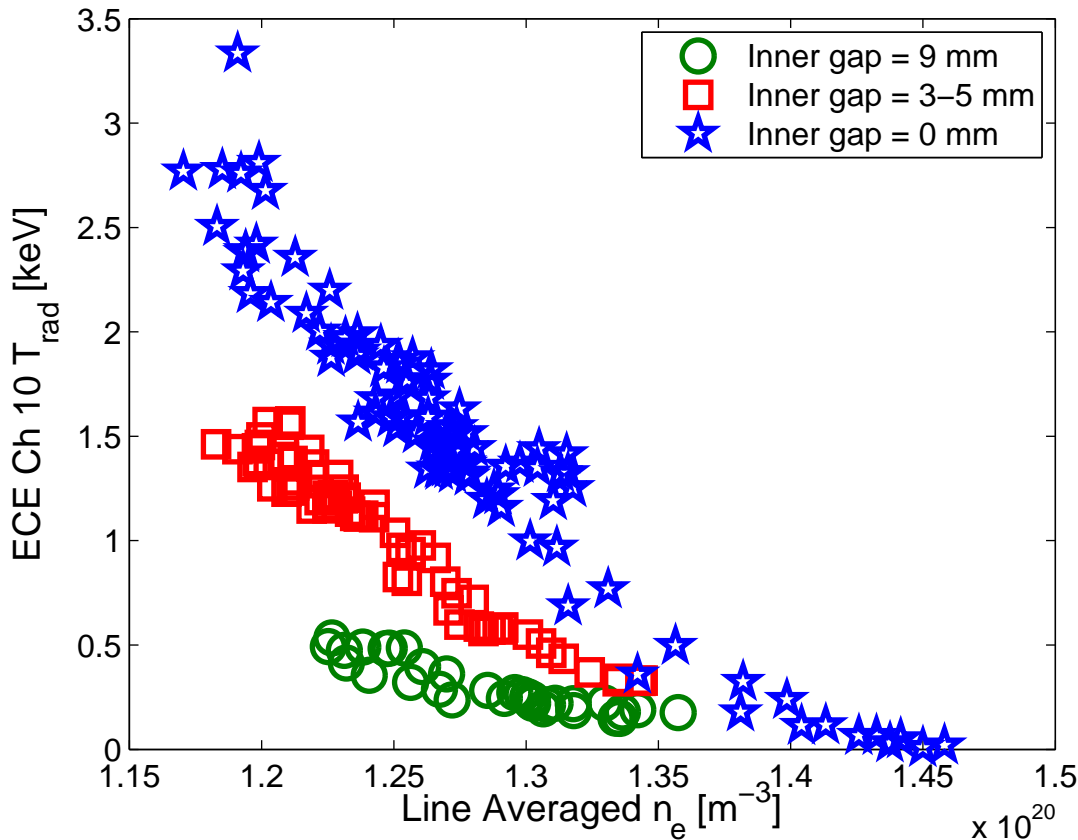


**Figure 6.** Comparison of non-thermal ECE as a function of density for different plasma-inner wall gaps. The frequency of ECE channel 10 maps to a major radius outside the LCFS. Thermal emission from before the LH turn on has been subtracted. All discharges plotted are at 800 kA and 5.4 T.

level. This increase in background makes direct comparison of ohmic and ICRF heated discharges difficult. Non-thermal ECE, which is not adversely effected by ICRF heating, is used for comparison instead. Figure 8 shows the non-thermal ECE as a function of density for L-mode discharges with varying ICRF power levels. A small increase in non-thermal emission is seen with increased ICRF power. Non-thermal emission in limited discharges is significantly higher than for ICRF heated, diverted discharges.

Results from the FTU LHCD experiment suggest that the LHCD density limit can be overcome by raising the temperature in the plasma edge ( $r/a > 0.8$ ) [18, 19]. The I-mode confinement regime on C-Mod consists of an H-mode like temperature pedestal at the plasma edge with an L-mode like density profile [20, 21, 22]. Comparing USN I-mode and USN L-mode discharges with similar density profiles and central temperatures provides a convenient way to assess the effect of edge temperature on the LHCD density limit. LHCD was applied to I-mode discharges ( $I_p = 900$  kA,  $P_{ICRF} = 2.8 - 3.8$  MW) with  $T_{e0} \sim 5$  keV and  $T_{r/a=0.9} = 500 - 800$  eV. The non-thermal ECE signatures increase

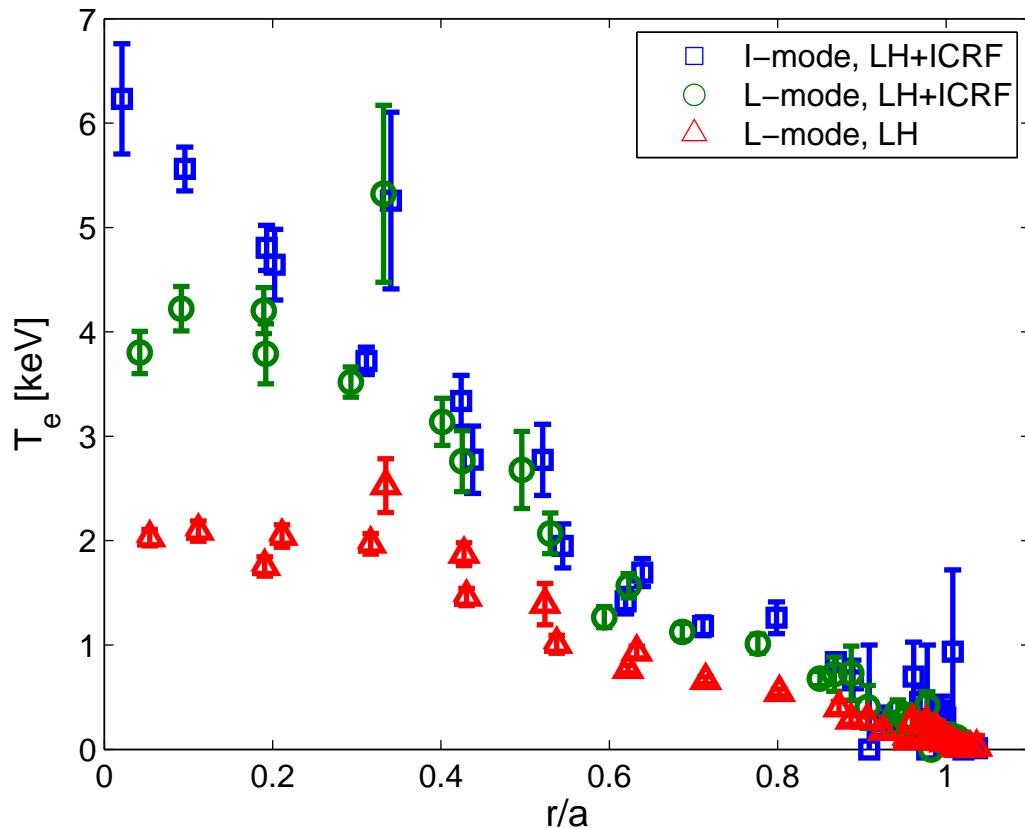


**Figure 7.** Comparison of electron temperature profiles measured by Thomson scattering in an L-mode discharge with LH and discharges with both LH and ICRH.

by a factor of  $\sim 2$  in I-mode as compared to L-modes with similar central temperatures (see Figure 9). This modest increase in non-thermal emission as edge temperature increases is smaller compared to the effect of changing between diverted and limited configurations. Thus, increasing edge  $T_e$  does not appear to eliminate the density limit for LHCD in a diverted tokamak, although it may increase absorption of waves which do penetrate past the LCFS.

## 5. Discussion and Conclusions

Simulations of parasitic collisional absorption in the SOL show that much of the absorption occurs in the region between the lower divertor and the mid-plane on the HFS [23]. The density at the inner wall is typically above the slow wave cutoff ( $n_e = 2.6 \times 10^{17} \text{ m}^{-3}$  at 4.6 GHz) even for large plasma-inner wall gaps ( $> 10 \text{ mm}$ ). The LH waves are able to propagate between the LCFS and the inner wall and parasitic collisional absorption may occur in this region. Operating in a regime with little (small plasma-inner wall gap) or no (inner wall limited) space for the waves to propagate

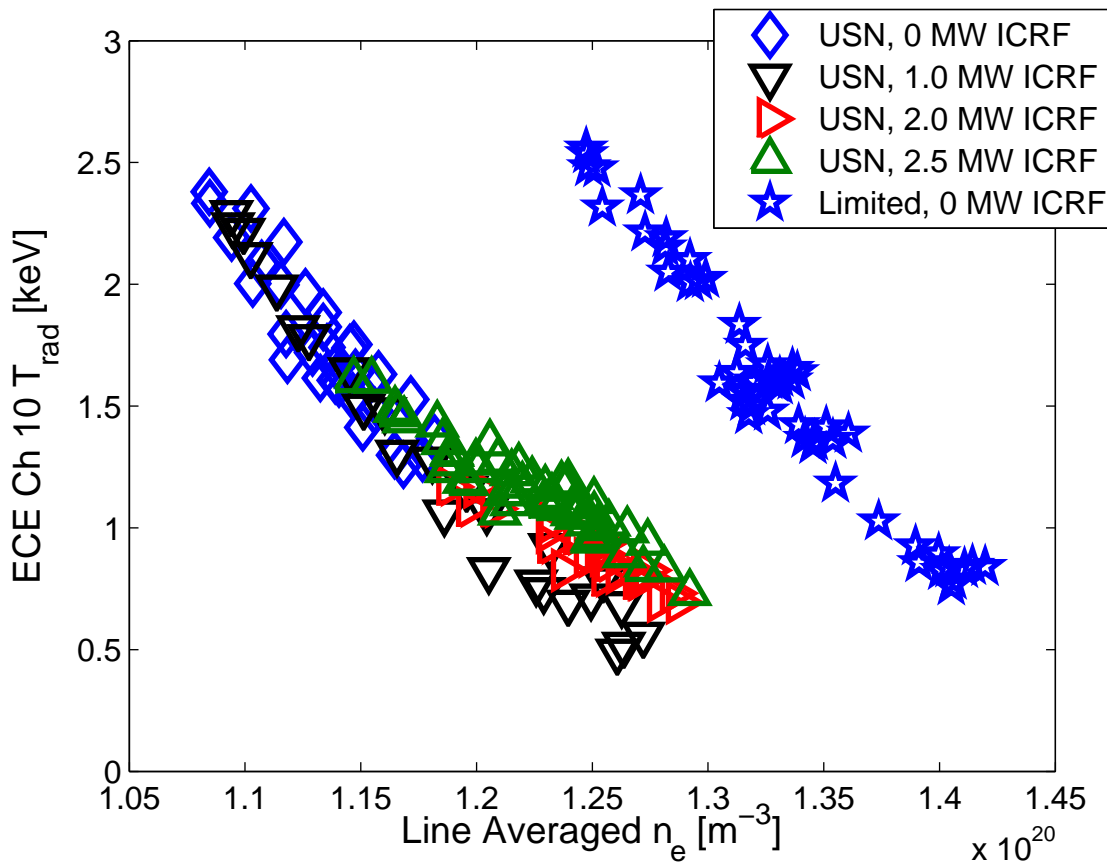


**Figure 8.** Comparison of non-thermal electron cyclotron emission as a function of density for different ICRF power levels. The frequency of ECE channel 10 maps to a major radius outside the LCFS. Thermal emission from before the LH turn on has been subtracted. All discharges plotted are at 1.1 MA, 5.4 T.

between the last closed flux surface and the conducting wall on the HFS may reduce or eliminate the parasitic losses in the SOL. Changes in the SOL behavior and neutral pressure as a result of the variation in plasma shape and position likely play an important role as well.

Discharges with large ( $> 10$  mm), small (3–5 mm), and zero (*i.e.* limited) plasma–inner wall gaps were simulated with the GENRAY/CQL3D ray tracing/Fokker-Planck code. The HXR synthetic diagnostic output is compared with experimental HXR data from these discharges in Figure 10. The synthetic diagnostic is in good agreement with experiment for the small and zero gap cases, but the synthetic diagnostic predicts a higher than observed count rate for the large gap case. This discrepancy may be due to the SOL model used in GENRAY. The model density profile in the SOL is based on an exponential decay of density away from the LCFS. Figure 3 shows that a simple exponential decay of the density is not an accurate representation of the experimental density profile. The SOL density profiles used for the large gap case were based on an

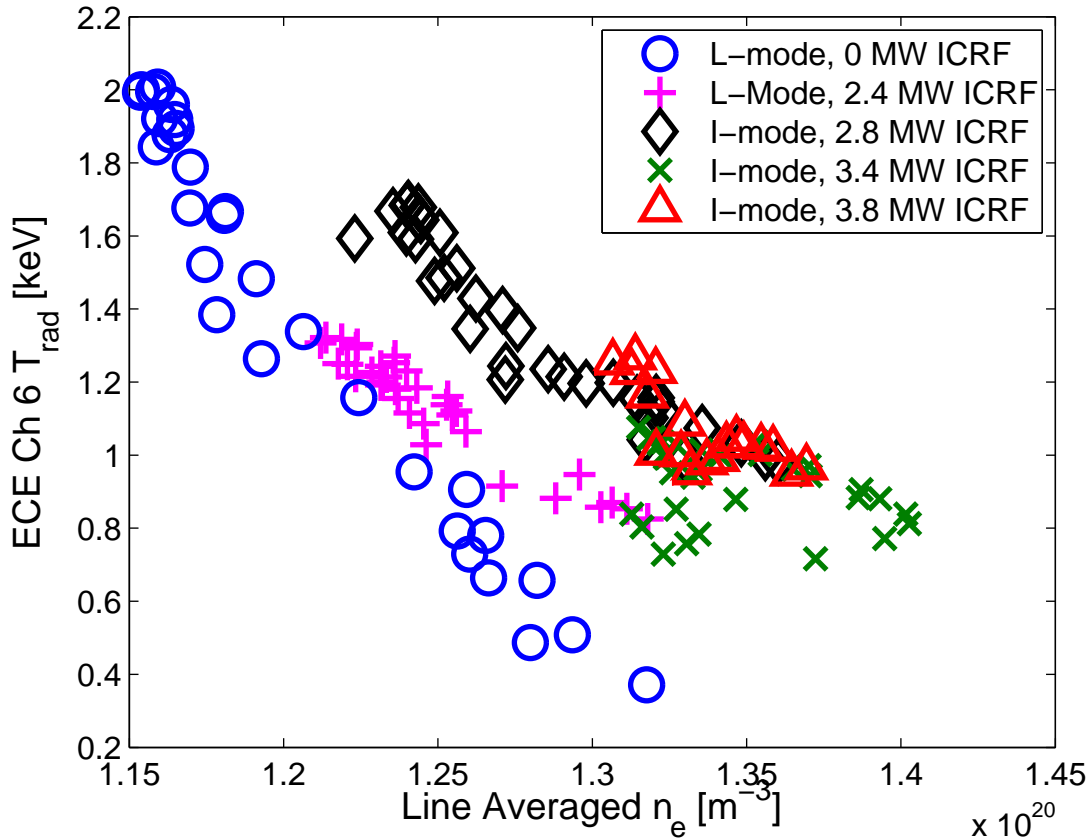


**Figure 9.** Comparison of non-thermal ECE as a function of density for L- and I-mode discharges at varying ICRF power levels. The frequency of ECE channel 6 maps to a major radius outside the LCFS. Thermal emission from before the LH turn on has been subtracted. All discharges plotted are at 900 kA, 5.6 T.

exponential fit of the reciprocating probe density profile for  $0 < \rho < 15$  mm. Rays may become trapped in the far SOL ( $\rho > 20$  mm) due to the change in the sign of the density gradient at  $\rho = 20 - 25$  mm, therefore increasing the amount of power damped in the SOL. Including the experimentally observed SOL profile in the model is a necessary step to understand the density limit for diverted configurations in detail.

Figure 11 shows the measured and predicted hard x-ray emission profiles for a high density ( $\bar{n}_e = 1.31 \times 10^{20} \text{ m}^{-3}$ ) inner wall limited discharge at 800 kA. Both the experiment and the synthetic diagnostic predict profiles which are peaked on axis, although the experimental values are slightly higher overall as compared to the model. This discrepancy may be due to thick target bremsstrahlung from energetic electrons striking the inner wall, which is not included in the synthetic diagnostic. Also, the simulation results do not include any radial diffusion of fast electrons, which would have the effect of smoothing out some of the structures seen in the synthetic diagnostic profile, and would also slightly increase the emission on the edge chords.

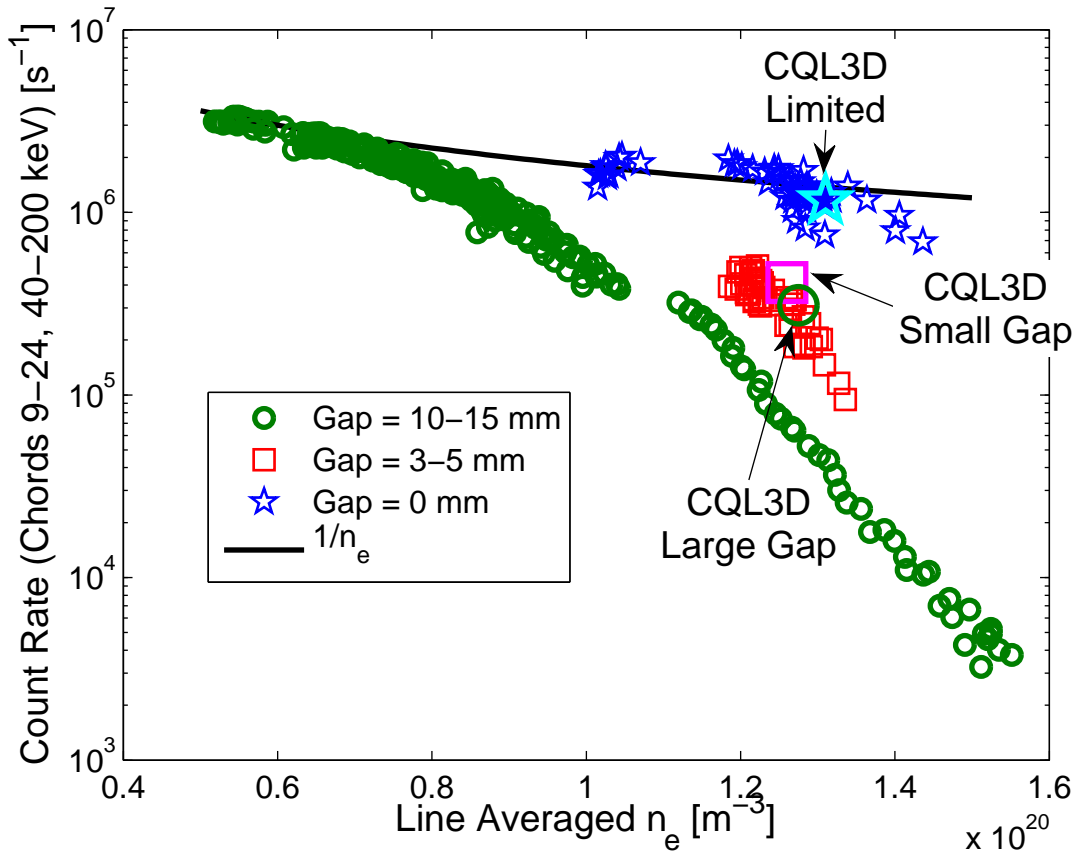


**Figure 10.** Comparison of measured and predicted hard x-ray emission at high density as a function of plasma–inner wall gap. Small points represent experimental data while large points represent synthetic diagnostic outputs from GENRAY/CQL3D.

Figure 12 shows the damped power as a function of  $n_{\parallel}$  for the three simulations described above (large inner gap, small inner gap, and zero inner gap). The small and zero inner gap cases show significantly more upshifting in  $n_{\parallel}$  before the rays are damped. The reason for the smaller upshift in the large inner gap case is that the rays are damped largely through collisional absorption, which is much less sensitive to  $n_{\parallel}$  than Landau damping. The simulations also show a shift in the power deposition radius as a function of plasma position. The power absorption profiles as a function of normalized radius are plotted in Figure 13 for the large, small, and zero inner gap simulations. For the large inner gap case only  $\sim 50\%$  of the power is absorbed inside the LCFS, while  $\sim 70\%$  and  $\sim 90\%$  of the power are absorbed inside the LCFS for the small and zero inner gap cases, respectively.

Although the strongest non-thermal electron signatures are observed in the limited configuration, limited discharges are of less interest to the C-Mod advanced scenarios program due to the difficulty in accessing high confinement regimes (H- and I-mode) without a diverted plasma. The increase in non-thermal emission in double null

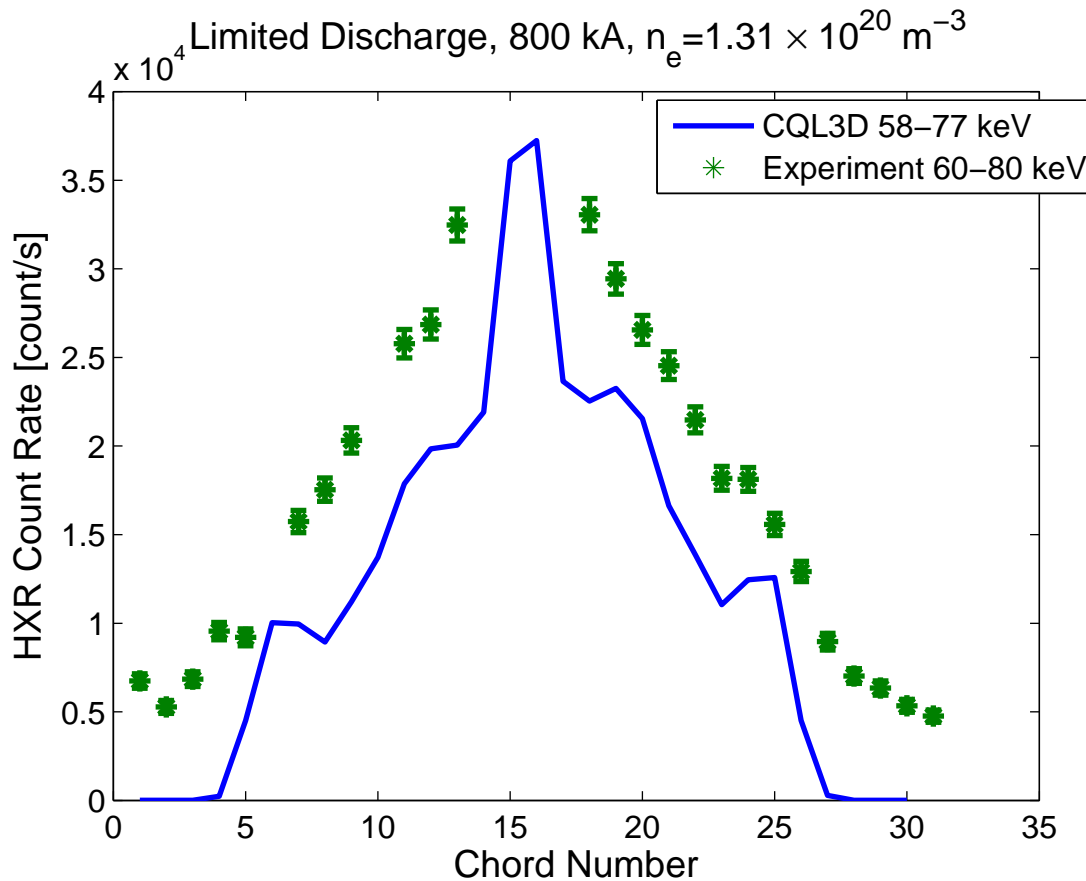


**Figure 11.** Comparison of measured and predicted hard x-ray emission profiles in a high density ( $\bar{n}_e = 1.31 \times 10^{20} \text{ m}^{-3}$ ) inner wall limited discharge. Thick target bremsstrahlung and emission from outside the LCFS are not included in the CQL3D synthetic diagnostic.

discharges, and also in single null discharges with small ( $< 5 \text{ mm}$ ) plasma–inner wall gaps, is encouraging and may be enhanced by operating in double null with a similarly small inner gap. Launching LH waves from the HFS wall of the tokamak may also increase the effectiveness of LHCD at high density, although constructing a LH launcher for the HFS presents considerable technical difficulties. Additional experimental and modeling work is necessary to identify the optimal conditions for LHCD at high density in a diverted configuration.

These results show a clear difference in the phenomenology of the LHCD density limit between diverted and limited configurations. Prior investigation of LHCD at such high densities was conducted in circular, limited tokamaks such as Alcator C [24] and FTU [25, 18, 19]. Although the experiments on C-Mod show no dependence on elongation, the difference between limited and diverted plasmas is significant and this may explain the unexpectedly low density limit encountered for diverted discharges in C-Mod. Future LHCD experiments in diverted, high-density discharges, such as



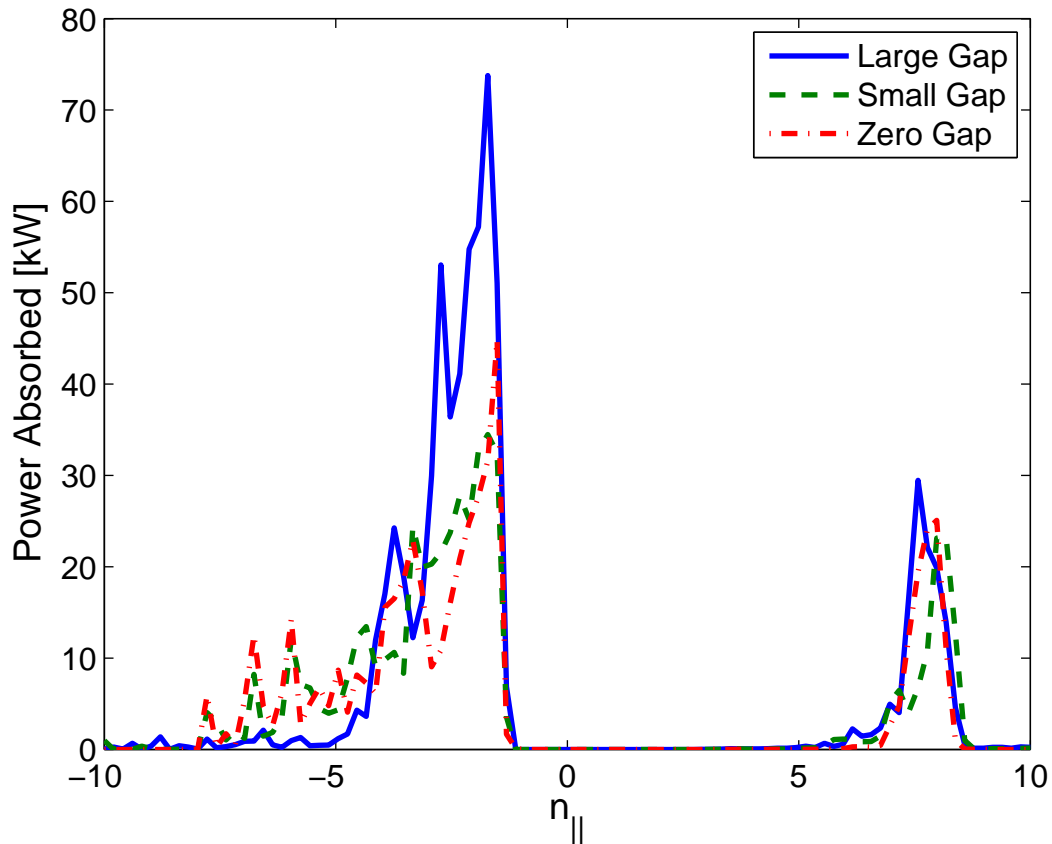


**Figure 12.** Comparison of simulated power absorption as a function of  $n_{||}$  for large inner gap, small inner gap, and zero inner gap discharges.

those anticipated for ITER [26, 27], need to be considered in the context of parasitic wave absorption in the SOL. Accurate predictions of the SOL temperature and density profiles, and possible modifications to the SOL profiles by the LH waves, will be necessary to properly assess the potential for parasitic absorption of LH waves outside the LCFS in future experiments.

### Acknowledgments

The authors would like to thank the C-Mod LHCD engineering team for their efforts. This work supported by USDOE awards DE-FC02-99ER54512 and DE-AC02-76CH03073.

### References

- [1] N. J. Fisch and A. H. Boozer. Creating an Asymmetric Plasma Resistivity with Waves. *Physical Review Letters*, 45(9):720–722, Sep 1980.
- [2] P. T. Bonoli, R. Parker, S. J. Wukitch, Y. Lin, M. Porkolab, J. C. Wright, E. Edlund, T. Graves,

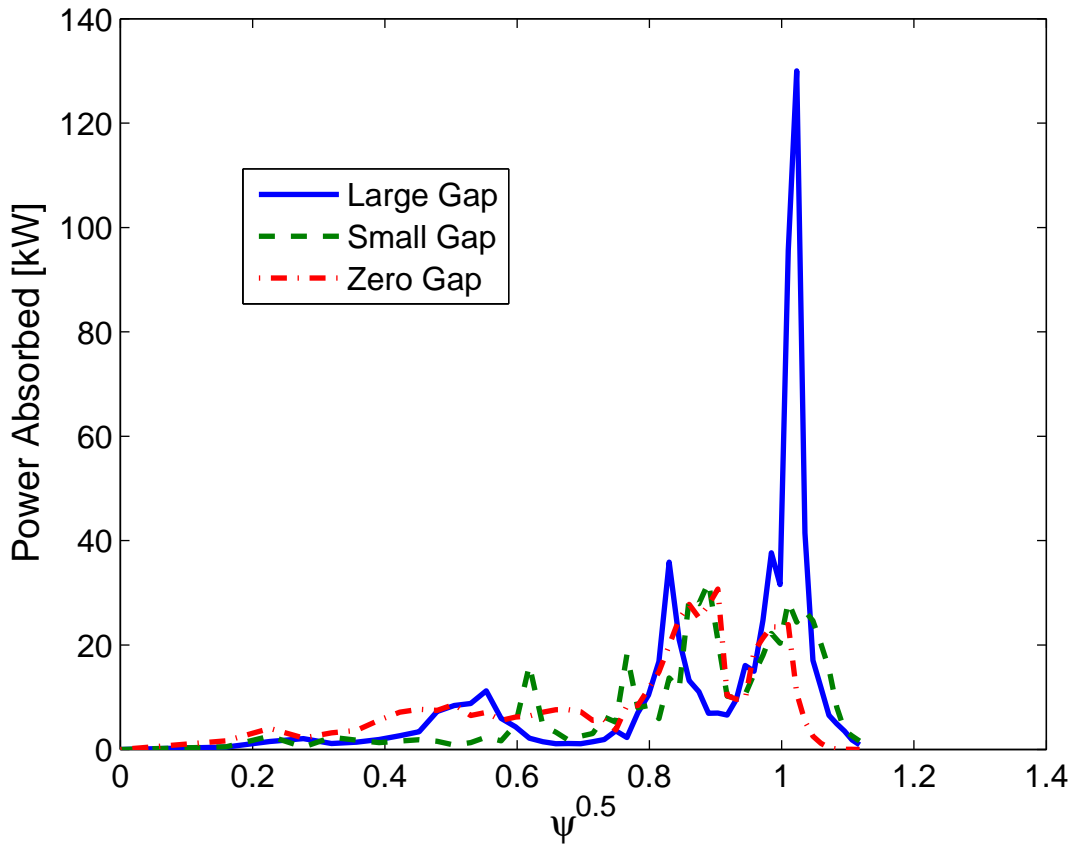


**Figure 13.** Comparison of simulated power absorption as a function of  $\psi^{0.5} \sim r/a$  for large inner gap, small inner gap, and zero inner gap discharges.

- L. Lin, J. Liptac, A. Parisot, A. E. Schmidt, V. Tang, W. Beck, R. Childs, M. Grimes, D. Gwinn, D. Johnson, J. Irby, A. Kanojia, P. Koert, S. Marazita, E. Marmor, D. Terry, R. Vieira, G. Wallace, J. Zaks, S. Bernabei, C. Brunkhorse, R. Ellis, E. Fredd, N. Greenough, J. Hosea, C. C. Kung, G. D. Loesser, J. Rushinski, G. Schilling, C. K. Phillips, J. R. Wilson, R. W. Harvey, C. L. Fiore, R. Granetz, M. Greenwald, A. E. Hubbard, I. H. Hutchinson, B. LaBombard, B. Lipschultz, J. Rice, J. A. Snipes, J. Terry, S. M. Wolfe, and the Alcator C-Mod Team. Wave-Particle Studies in the Ion Cyclotron and Lower Hybrid Ranges of Frequencies in Alcator C-Mod. *Fusion Science and Technology*, 51(3):401–436, April 2007.
- [3] I. H. Hutchinson, R. Boivin, F. Bombarda, P. Bonoli, S. Fairfax, C. Fiore, J. Goetz, S. Golovato, R. Granetz, M. Greenwald, S. Horne, A. Hubbard, J. Irby, B. LaBombard, B. Lipschultz, E. Marmor, G. McCracken, M. Porkolab, J. Rice, J. Snipes, Y. Takase, J. Terry, S. Wolfe, C. Christensen, D. Garnier, M. Graf, T. Hsu, T. Luke, M. May, A. Niemczewski, G. Tinios, J. Schachter, and J. Urbahn. First results from Alcator C-MOD. *Physics of Plasmas*, 1(5):1511–1518, 1994.
- [4] J.R. Wilson, R. Parker, M. Bitter, P.T. Bonoli, C. Fiore, R.W. Harvey, K. Hill, A.E. Hubbard, J.W. Hughes, A. Ince-Cushman, C. Kessel, J.S. Ko, O. Meneghini, C.K. Phillips, M. Porkolab, J. Rice, A.E. Schmidt, S. Scott, S. Shiraiwa, E. Valeo, G. Wallace, J.C. Wright, and the Alcator C-Mod Team. Lower hybrid heating and current drive on the Alcator C-Mod tokamak. *Nuclear Fusion*, 49(11):115015, 2009.
- [5] G. M. Wallace, R. R. Parker, P. T. Bonoli, A. E. Schmidt, D. G. Whyte, J. R. Wilson, and S. J.

- Wukitch. Interaction of Lower Hybrid Waves with the Scrape Off Layer. *Bull. Am. Phys. Soc.*, 53(14):222, November 2008.
- [6] G. M. Wallace, R. R. Parker, P. T. Bonoli, R. W. Harvey, A. E. Schmidt, A. P. Smirnov, D. G. Whyte, J. R. Wilson, J. C. Wright, and S. J. Wukitch. Observations of lower hybrid wave absorption in the scrape off layer of a diverted tokamak. In Volodymyr Bobkov and Jean-Marie Noterdaeme, editors, *RADIO FREQUENCY POWER IN PLASMAS: Proceedings of the 18th Topical Conference*, volume 1187, pages 395–398. American Institute of Physics, Melville, NY, 2009.
- [7] G. M. Wallace, R. R. Parker, P. T. Bonoli, A. E. Hubbard, J. W. Hughes, B. L. LaBombard, O. Meneghini, A. E. Schmidt, S. Shiraiwa, D. G. Whyte, J. C. Wright, S. J. Wukitch, R. W. Harvey, A. P. Smirnov, and J. R. Wilson. Absorption of lower hybrid waves in the scrape off layer of a diverted tokamak. *Physics of Plasmas*, 17(8):082508, 2010.
- [8] M Goniche, L Amicucci, Y Baranov, V Basiuk, G Calabro, A Cardinali, C Castaldo, R Cesario, J Decker, D Dodt, A Ekedahl, L Figini, J Garcia, G Giruzzi, J Hillairet, G T Hoang, A Hubbard, E Joffrin, K Kirov, X Litaudon, J Mailloux, T Oosako, R Parker, V Pericoli Ridolfini, Y Peysson, P Platania, F Rimini, P K Sharma, C Sozzi, and G Wallace. Lower hybrid current drive for the steady-state scenario. *Plasma Physics and Controlled Fusion*, 52(12):124031, 2010.
- [9] W. Hooke. Review of experiments on current drive in Tokamaks by means of RF waves. *Plasma Physics and Controlled Fusion*, 26(1A):133–144, 1984.
- [10] Y. Takase, M. Porkolab, J. J. Schuss, R. L. Watterson, C. L. Fiore, R. E. Slusher, and C. M. Surko. Observation of parametric instabilities in the lower-hybrid range of frequencies in the high-density tokamak. *Physics of Fluids*, 28(3):983–994, 1985.
- [11] J. Liptac, R. Parker, V. Tang, Y. Peysson, and J. Decker. Hard x-ray diagnostic for lower hybrid experiments on Alcator C-Mod. *Review of Scientific Instruments*, 77(10):103504, 2006.
- [12] A. P. Smirnov and R.W. Harvey. *Bull. Am. Phys. Soc.*, 40:1837, 1995.
- [13] R. W. Harvey and M. McCoy. The CQL3D Fokker-Planck Code. In *Proceedings of the IAEA Technical Committee Meeting on Simulation and Modeling of Thermonuclear Plasmas*, pages 489–526, 1992.
- [14] R.W. Harvey and M.G. McCoy. The CQL3D Fokker-Planck Code. Technical report, General Atomics, 1992.
- [15] N. J. Fisch. Theory of current drive in plasmas. *Reviews of Modern Physics*, 59:175–234, January 1987.
- [16] G. M. Wallace et al. Lower hybrid current drive studies on Alcator C-Mod. To be submitted to *Nuclear Fusion*, 2011.
- [17] Paul T. Bonoli and Ronald C. Englade. Simulation model for lower hybrid current drive. *Physics of Fluids*, 29(9):2937–2950, 1986.
- [18] R. Cesario, L. Amicucci, G. Calabrò, A. Cardinali, C. Castaldo, M. Marinucci, L. Panaccione, V. Pericoli-Ridolfini, A. A. Tuccillo, and O. Tudisco. Lower hybrid current drive at ITER-relevant high plasma densities. In Volodymyr Bobkov and Jean-Marie Noterdaeme, editors, *RADIO FREQUENCY POWER IN PLASMAS: Proceedings of the 18th Topical Conference*, volume 1187, pages 419–422. American Institute of Physics, Melville, NY, 2009.
- [19] R. Cesario, L. Amicucci, A. Cardinali, C. Castaldo, M. Marinucci, L. Panaccione, F. Santini, O. Tudisco, M.L. Apicella, G. Calabr, C. Cianfarani, D. Frigione, A. Galli, G. Mazzitelli, C. Mazzotta, V. Pericoli, G. Schettini, and A.A. Tuccillo. Current drive at plasma densities required for thermonuclear reactors. *Nat. Commun.*, 1:55, 2010.
- [20] A. E. Hubbard et al. I-mode. Submitted to *Physics of Plasmas*, 2010.
- [21] D.G. Whyte, A.E. Hubbard, J.W. Hughes, B. Lipschultz, J.E. Rice, E.S. Marmor, M. Greenwald, I. Cziegler, A. Dominguez, T. Golfinopoulos, N. Howard, L. Lin, R.M. McDermott, M. Porkolab, M.L. Reinke, J. Terry, N. Tsujii, S. Wolfe, S. Wukitch, Y. Lin, and the Alcator C-Mod Team. I-mode: an h-mode energy confinement regime with l-mode particle transport in alcator c-mod. *Nuclear Fusion*, 50(10):105005, 2010.

- [22] R. M. McDermott, B. Lipschultz, J. W. Hughes, P. J. Catto, A. E. Hubbard, I. H. Hutchinson, R. S. Granetz, M. Greenwald, B. LaBombard, K. Marr, M. L. Reinke, J. E. Rice, and D. Whyte. Edge radial electric field structure and its connections to h-mode confinement in alcator c-mod plasmas. *Physics of Plasmas*, 16(5):056103, 2009.
- [23] J. R. Wilson, C. Kessel, S. Scott, E. Valeo, R. R. Parker, P. T. Bonoli, A. E. Hubbard, J. W. Hughes, J. S. Ko, O. Meneghini, M. Porkolab, J. E. Rice, A. E. Schmidt, S. Shiraiwa, G. M. Wallace, and J. C. Wright. Analysis and scenario modeling of LHCD on Alcator C-Mod. *Bull. Am. Phys. Soc.*, page 8007, November 2009.
- [24] M. Porkolab, J. J. Schuss, B. Lloyd, Y. Takase, S. Texter, P. Bonoli, C. Fiore, R. Gandy, D. Gwinn, B. Lipschultz, E. Marmor, D. Pappas, R. Parker, and P. Pribyl. Observation of Lower-Hybrid Current Drive at High Densities in the Alcator C Tokamak. *Physical Review Letters*, 53(5):450–453, Jul 1984.
- [25] V. Pericoli-Ridolfini, E. Barbato, S. Cirant, H. Kroegler, L. Panaccione, S. Podda, F. Alladio, B. Angelini, M. L. Apicella, G. Apruzzese, L. Bertalot, A. Bertocchi, M. Borra, G. Bracco, A. Bruschi, G. Buceti, P. Buratti, A. Cardinali, C. Centioli, R. Cesario, S. Ciattaglia, V. Cocilovo, F. Crisanti, R. De Angelis, F. De Marco, B. Esposito, and D. Frigione. High Plasma Density Lower-Hybrid Current Drive in the FTU Tokamak. *Physical Review Letters*, 82(1):93–96, Jan 1999.
- [26] R. Aymar, P. Barabaschi, and Y. Shimomura. The ITER design. *Plasma Physics and Controlled Fusion*, 44:519–565, May 2002.
- [27] G.T. Hoang, A. Bcoulet, J. Jacquinet, J.F. Artaud, Y.S. Bae, B. Beaumont, J.H. Belo, G. Bergerby, Joo P.S. Bizarro, P. Bonoli, M.H. Cho, J. Decker, L. Delpech, A. Ekedahl, J. Garcia, G. Giruzzi, M. Goniche, C. Gormezano, D. Guilhem, J. Hillairet, F. Imbeaux, F. Kazarian, C. Kessel, S.H. Kim, J.G. Kwak, J.H. Jeong, J.B. Lister, X. Litaudon, R. Magne, S. Milora, F. Mirizzi, W. Namkung, J.M. Noterdaeme, S.I. Park, R. Parker, Y. Peysson, D. Rasmussen, P.K. Sharma, M. Schneider, E. Synakowski, A. Tanga, A. Tuccillo, and Y.X. Wan. A lower hybrid current drive system for ITER. *Nuclear Fusion*, 49(7):075001, 2009.